International Journal of Civil Engineering
https://doi.org/10.1007/s40999-026-01213-5

RESEARCH PAPER

Compressive Behavior of Reinforced Concrete Pedestals with Corroded Steel Reinforcements

Giuseppe Campione[1] · **Michele Fabio Granata**[1] · **Francesco Cannella**[1]

Received: 26 February 2024 / Revised: 28 March 2025 / Accepted: 20 February 2026

Abstract
The behavior of concrete pedestals for the transmission of loads from bridge deck to substructure is investigated till failure. An experimental campaign with 24 prismatic pedestals tested in compression was carried out with different heights/width ratios and percentages of steel reinforcement at the bottom edge. Corrosion of the lower reinforcements was induced to simulate the behavior of pedestals of existing bridges, by placing specimens in a tank with sodium chloride producing a pitting attack. The effective potential measurements, the tensile tests on the reinforcing bars (corroded and non-corroded) and the compressive tests on the pedestals show that the compressive strength of these elements is governed mainly by the geometric properties, but it is not significantly affected by the corrosion of the lower bars. Analytical models for strength assessment have to be diversified by considering plate type, and punched-governed or classic strut-and-tie models depending on the actual behavior at failure. The results show that the reduction in strength by corrosion is more evident in the lower specimens, with a reduction of the ultimate load of about 12%. The strut-and-tie model can be used effectively for heights equal to or greater than the element width, taking into account the variation of stress fields for tall pedestals, while punching and flexural models are more reliable for lower pedestals. Numerical FE models with nonlinear analyses confirm the results obtained with experimental tests and analytical methods.

Keywords Pedestals · Reinforced concrete · Bridges: Bearing supports · Corrosion · Strut-and-tie model

1 Introduction

The deck of a viaduct consists of several structural components (see Fig. 1). These include girders made of either reinforced concrete (RC) or prestressed reinforced concrete (PRC) beams and slabs. The piers often present bent caps (or abutment-top beams), which are deep beams located at the top of the substructures. Pier crossheads, which support the girders and host the bearings of each deck element, are placed transversely to the bridge centerline. Between the beams and the piers, there are support devices that can be bearings or seismic isolators. Additionally, between the support devices and the pier crossheads, reinforced concrete elements are placed in the form of prismatic blocks (pedestals). These blocks enable the deck to achieve the desired transverse slope and transfer the upper girder loads to the deep beams below.

In steel girders pedestals can be made of concrete or steel and their role in countering seismic effects was investigated in [1], while the failure modes according to the type of bearing support were considered in [2] and [3]. Figure 2 presents pictures of pedestals with different configurations, corresponding to common types of bridge decks, showing the position and function of pedestals as intermediate connecting elements between bearing supports and deep beams of substructure [4]. Figure 2a and b show pedestals of varying heights that are used to achieve the transverse slope required for the proper positioning of bearing supports. Figure 2c and d depict elastomeric bearings located between pedestals and girders.

From a structural point of view, pedestals are typically monolithic elements predominantly constructed from

✉ Giuseppe Campione
giuseppe.campione@unipa.it

Michele Fabio Granata
michelefabio.granata@unipa.it

Francesco Cannella
f.cannella@stradeanas.it

[1] Department of Engineering, University of Palermo, Viale delle Scienze, 90128 Palermo, Italy

Published online: 30 March 2026

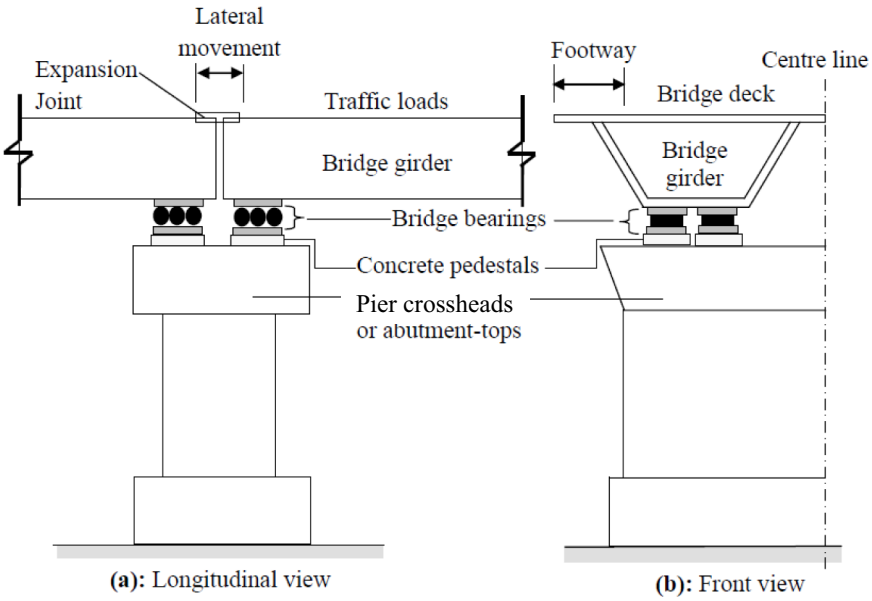

Fig. 1 Concrete pedestals for bridge girder bearings

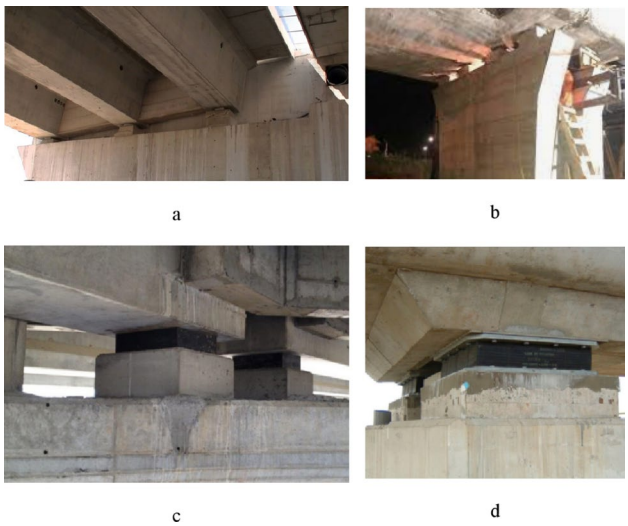

Fig. 2 Examples of support beams for reinforced concrete bridge beams. **a** and **b** Pedestals with different heights for transverse slope; **c** and **d** pedestals under elastomeric bearings with different width/depth ratios

high-strength reinforced concrete, often exceeding the strength of piers. Their primary function, as previously mentioned, includes establishing support surfaces for restraint devices, creating varying levels for bearing placements on each beam, accommodating clamps or bars to secure support devices on crossbeams, and compensating for construction errors.

Loads transmitted from the deck to the pedestals through the supports are mainly vertical forces (centered or eccentric) from dead and live loads, as well as horizontal forces resulting from short-term effects such as earthquakes, braking, moving loads, and temperature fluctuations, along with long-term effects like creep and shrinkage.

Pedestals are generally cast in a subsequent phase after the construction of piers, bent caps, and abutments, requiring careful execution due to their critical role. In some cases, high-quality rheoplastic mortars are employed to ensure precise leveling of bearing supports and minimize local shrinkage effects. Their height varies from a few centimeters to over 50 cm, or sometimes more, and they typically house bearing devices at their tops, often composed of elastomeric pads capable of transferring both vertical and horizontal loads avoiding localized failures in substructures. Figure 3 illustrates a cross-section of a pedestal with typical reinforcement layouts.

To withstand the stress induced by the supported girder, a reinforcing cage with multiple layers of steel reinforcements is often adopted. Typically, the most critical layer is positioned at the bottom of the cage, as it bears the highest transverse tension resulting from axial compression exerted by the bearings. Additionally, to address horizontal forces, connection brackets or studs are often embedded in the deep beams, specifically designed to resist pure shear.

An evaluation of the behavior of concrete pedestals under compressive loads is reported in [5] and [6], emphasizing the local failure of these concrete blocks with loads acting on reduced areas. The reinforcement arrangement and the confinement effect in concrete pedestals was investigated in [7] comparing the failure of unreinforced blocks with those reinforced only laterally, but the contribution of high quantities of bottom reinforcement was not considered.

In many bridges, the degradation of steel reinforcement due to corrosion, often caused by concrete carbonation or chloride attack, leads to a reduction in reinforcement area and the consequences on the structural behavior can be significantly increased if degradation affects squat

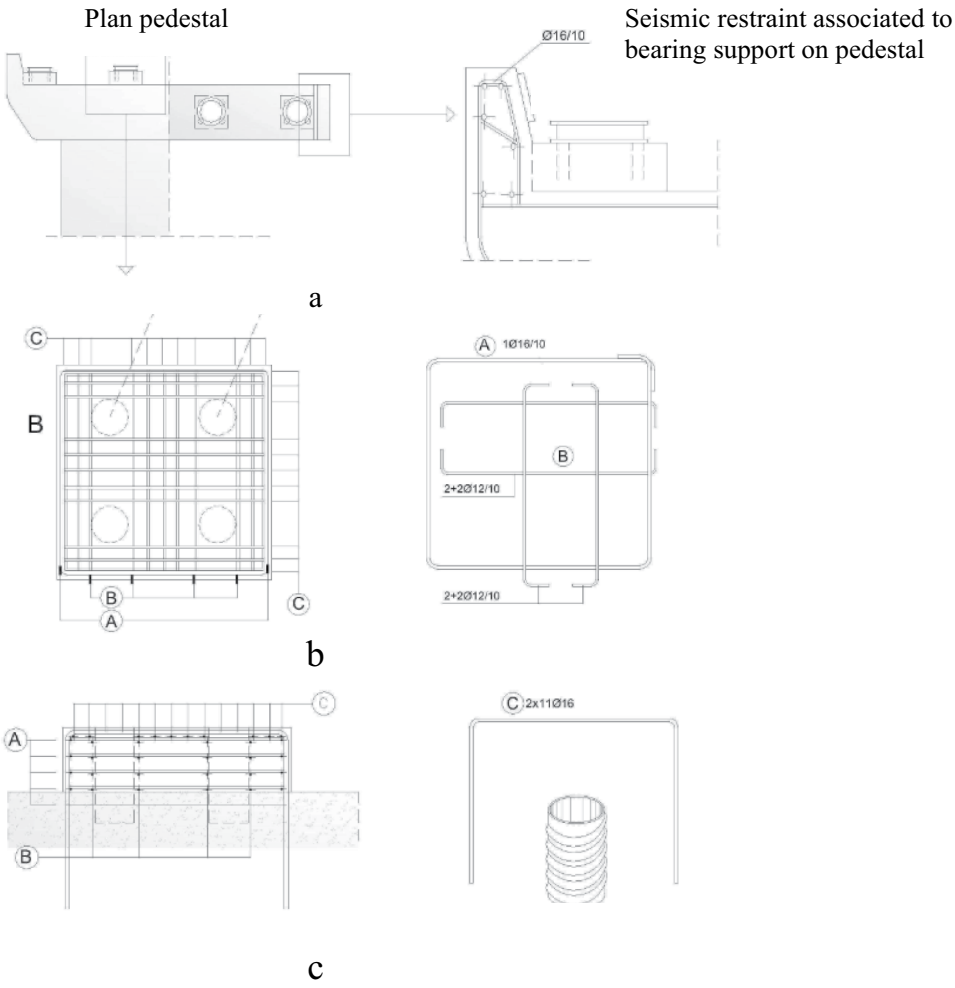

Fig. 3 Typical reinforcement arrangements of pedestals. **a** Drawings of bearing supports with pedestals and seismic restraints on a pier or abutment; **b** plan view of pedestal with typical reinforcement arrangement; **c** side view of reinforcement arrangement

Fig. 4 Examples of corrosion degradation of pedestals

elements and disturbed regions, such as half-joints [8–9]. This deterioration is compounded by the formation of split cracks on pedestal faces, resulting from the expansion of corroded bars. These issues jointly could diminish the load-bearing capacity of pedestals, particularly when cracking affects areas under compression and the confinement reinforcements are so degraded that they are no longer effective. This situation may also arise directly from the maintenance conditions and from the state of the upper bearings, as well as from the modality of load transfer from the girder to the pier or abutment crosshead, as noted by inspections of existing bridges [10].

Figure 4 illustrates several instances of pedestal damage caused by corroded reinforcing bars (see Fig. 4a, c), improper sizing (see Fig. 4b), or incorrect positioning and insufficient reinforcement with resistance entrusted only to high-strength mortar (see Fig. 4d). These issues can make the viaduct non-operational, reaching a Service Limit State, and in severe cases, they can cause significant damage to the superstructures, with loss of support, unexpected bearing settlements or sudden rotations till Ultimate Limit State [11]. It can be observed that, in most cases, draining water

from the deck damages the lateral surfaces of the pedestal and, consequently, the confinement reinforcements, also causing spalling and deterioration of the concrete. In some cases, such as that shown in Fig. 4d, confidence is placed solely in high-strength mortars, creating low pedestals without reinforcement, which can lead to sudden brittle failures of these elements through mechanisms similar to those studied in [7]. Conversely, when horizontal grid reinforcement is provided in the bottom edge of the pedestal, this is less exposed to corrosion and establishes a failure mechanism in which compressed concrete and lower steel in tension cooperate. This is the most common case and will be further developed in the following sections, considering that the compressive forces are often accompanied by significant shear forces resulting from the horizontal forces transmitted to the block by the bearing devices and vertical studs [12].

This study investigates, both theoretically and experimentally, the behavior of pedestals exposed to corrosion phenomena on the bottom reinforcement, focusing on the compressive response of these elements by varying the height/width ratio, that is by maintaining a fixed base dimension and a variable block height, with different percentages of reinforcement.

In fact, the compressive response of pedestals significantly depends on geometric ratios, particularly height and reinforcement percentage. The choice of the specimens for the experimental investigation takes into account the most common properties of actual pedestals in existing concrete bridges and the literature studies about the size effect [13], in order to have reliable results of tests and useful results to be used for practice engineering applications. The predominant behavior is governed by the longitudinal and transverse strength mechanism established within the concrete block, where compressive stresses from the upper bearing support spread to the underside of the pedestal and subsequently to the substructure element (pier or abutment) hosting it. This mechanism can be effectively understood through structural models like strut-and-tie ones, which require experimental validation as geometric properties vary.

This study thus combines experimental testing, where the primary parameter varied is the ratio between the geometric properties of the concrete block, alongside the conditions of the lower main reinforcement, which may undergo corrosion, coupled with concrete deterioration due to ageing of the support element and rendering ineffective the confinement of reinforcement because of its absence or deterioration.

The following sections will outline the experimental campaign and interpret the results using appropriate strut-and-tie models, which are differentiated based on the predominant mechanism observed. Finally, validation through Finite Element models and non-linear analyses is carried out.

2 Experimental Campaign

2.1 Specimen Description and Test Set-Up

The experimental research aimed to assess the mechanical behavior of concrete pedestals, up to failure, in the absence or presence of corrosion of the bottom reinforcement. In particular, 24 prismatic reinforced concrete elements were tested, all featuring a square base with a side length $B = 400$ mm and heights $H = 200$, 300, and 400 mm. The specimens were reinforced with 4 bars in the lower area in both the longitudinal and transverse directions, varying in diameter ϕ: 10 mm, 12 mm, 14 mm, and 16 mm. Table 1 presents the identification code of the samples, the dimensions of the pedestals, and the geometric and mechanical reinforcement ratios defined as $\rho = \frac{A_f}{B \cdot H}$ and $\omega = \rho \frac{f_y}{f_c}$, A_f being the area of the steel bars, B and H the base and height of the pedestal, f_c the cylindrical concrete strength and f_y the yield stress of the bars. The choice of geometric ratios was made to achieve low pedestals with $H/B = 0.5$, medium pedestals with $H/B = 0.75$, and high pedestals with $H/B = 1$.

Table 1 Geometrical properties of specimens

Specimen	B (mm)	H (mm)	*n*. bars	φ (mm)	A_f (mm^2)	ρ	ω	fy (MPa)	fc (MPa)
1	400	200	4	10	314.0	0.003925	0.0340167	390	45
2	400	200	4	12	452.2	0.005652	0.048984	390	45
3	400	200	4	14	615.4	0.007693	0.0666727	390	45
4	400	200	4	16	803.8	0.010048	0.0870827	390	45
5	400	300	4	10	314.0	0.0026167	0.0226778	390	45
6	400	300	4	12	452.2	0.003768	0.032656	390	45
7	400	300	4	14	615.4	0.0051287	0.0444484	390	45
8	400	300	4	16	803.8	0.0066987	0.0580551	390	45
9	400	400	4	10	314.0	0.0019625	0.0170083	390	45
10	400	400	4	12	452.2	0.002826	0.024492	390	45
11	400	400	4	14	615.4	0.0038465	0.0333363	390	45
12	400	400	4	16	803.8	0.005024	0.0435413	390	45

Fig. 5 Construction phase of samples

a b

Fig. 6 Corrosion of reinforcement. **a** Specimens in the tank of water solution with sodium chloride; **b** pitting corrosion of reinforcing bars due to chloride attack

Regarding the reinforcements, the range investigated included total lower reinforcement percentages in both directions (2ρ) from 0.4% to 2%, which appeared representative of the most common situations for lightly or heavily reinforced blocks.

Figure 5 depicts a construction phase of the samples, illustrating the reinforcements arranged in the two orthogonal horizontal directions. The ends of the reinforcements with different diameters are hooked to prevent failures due to bond loss.

To induce artificial corrosion through chloride exposure (which can cause pitting rather than uniform corrosion along the bars), the pedestals were immersed, as shown in Fig. 6, in a solution of water and sodium chloride (35 g per liter) for a duration of 270 days. Figure 6a illustrates the tanks utilized to submerge the specimens in a saline solution, thus facilitating the corrosion process. This procedure aimed to simulate corrosion conditions similar to those experienced by structures exposed to marine environments and shown in Fig. 6b, following methods described in the literature, such as by Yohai et al. [14]. The use of sodium chloride induces a localized pitting effect that reduces the effective cross-sectional area of the reinforcing bars.

Before immersing the specimens and measuring the corrosion potential, the exposed steel bars were properly cleaned to remove any surface rust that may have formed during the preceding 10-day exposure period. The trend of the corrosion potential was measured using a voltmeter, as depicted in Fig. 7a. This instrument allows for measurement of the electrical potential difference between two points in a circuit, referencing a Cu/CuSO4 (Copper/Copper Sulphate) electrode with a potential of 0.34 V vs. SHE (Standard Hydrogen Electrode). The unit of measurement is volts.

To ensure accurate potential measurements and avoid artifacts due to the presence of water in the solution, the potential values were measured on a sponge soaked in the solution, as recommended in [15] and compared directly with measurements taken in direct contact with the solution. The potential values were monitored periodically, ensuring that they fell below the corrosion initiation threshold of -0.5 mV to confirm the onset of corrosion. As shown in Figs. 7b, c, and d, the measured potential values indicate that the corrosion process of the reinforcing bars activated and propagated over a period ranging from 30 to 60 days.

Obviously, artificially induced corrosion differs from natural corrosion, and the literature contains several studies correlating the two phenomena [16]. These studies also indicate the current density to be used in artificial corrosion (an accepted value is approximately 100 μA/cm²) to ensure that the characteristics at the concrete interface and the cracking patterns do not significantly differ from those observed in natural corrosion, although data and studies on natural corrosion are limited [17]. From this perspective, the chloride immersion tank method provides appreciable results [15], especially when the aim is to provide pitting rather than uniform corrosion. Reference to studies on corrosion of reinforcements and its significance in term of strength and ductility or bond reduction can be found in the works of Andrade [18] or Imperatore et al. [19].

2.2 Mechanical Characterization of Materials

For the mechanical characterization of the materials, uniaxial tensile tests on the reinforcing bars were carried out together with compression tests on cores extracted from pedestal samples. The compression tests on these cores supplied strength values of 43 MPa, 45 MPa, and 47 MPa, averaging f_c = 45 MPa.

Additionally, two corroded and two non-corroded steel bars were tested, with diameters of 12 mm and 14 mm for each type. These bars were extracted from specimens not used for structural testing.

Table 2 supplies the mechanical properties of the bars. Here, d_{nom} denotes the equivalent diameter of the bar, A represents its cross-sectional area, f_y and f_u indicate the yielding and ultimate stresses respectively, while ε_g signifies the corresponding strain at failure. It was found that the reduction

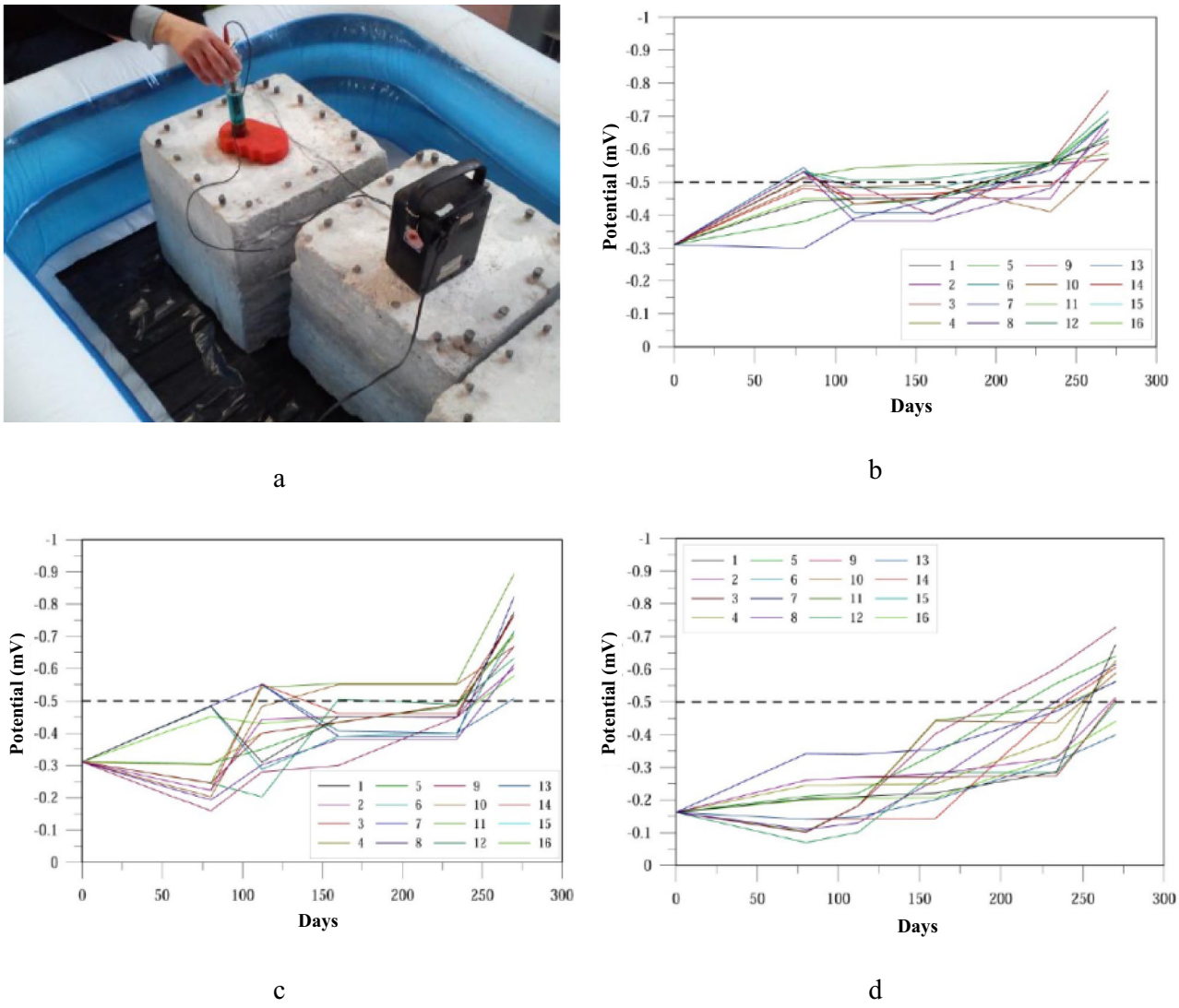

Fig. 7 Corrosion procedure. **a** Sample in the tank and measure of potential. Average potential value for beams with height: **b** 200 **c** 300 and **d** 400 mm

Table 2 Results of tensile tests on steel bars

Specimen	d_{nom} [mm]	A [mm^2]	f_y [MPa]	f_t [MPa]	ε_g [%]
FE12NC	12	113	400	429	11
FE12C	12	109	380	408	10
FE14NC	14	154	400	465	13
FE14C	14	152	397	467	13

in area (and consequently in corresponding mass) of the corroded bars ranges between 3% and 7%.

Figure 8 shows the results relating to the tests carried out on corroded and non-corroded bars with a diameter of 12 and 14 mm. Based on the results obtained, it is possible to observe that the corrosion of the bar led to a very limited reduction in yielding stress and ultimate stress and a small reduction of ductility of about 5% only in the bar with d_{nom} = 12 mm, which was also the most corroded one with mass loss of 7%.

The test results on the bars from the experimental campaign are consistent with the database provided by Imperatore et al. [19], which reports a maximum strength reduction between 5% and 10% for the aforementioned mass loss due to corrosion. These results for the steel bars influence the global behavior of the pedestal, as will be seen later, where an increase in localized stress due to pitting does not significantly reduce the overall load-bearing capacity of the pedestal, because the reduction of steel mechanical properties is limited.

2.3 Compressive Tests on Pedestals

This section presents experimental results from centered compression tests conducted on samples with varying reinforcement quantities and corrosion levels. Each

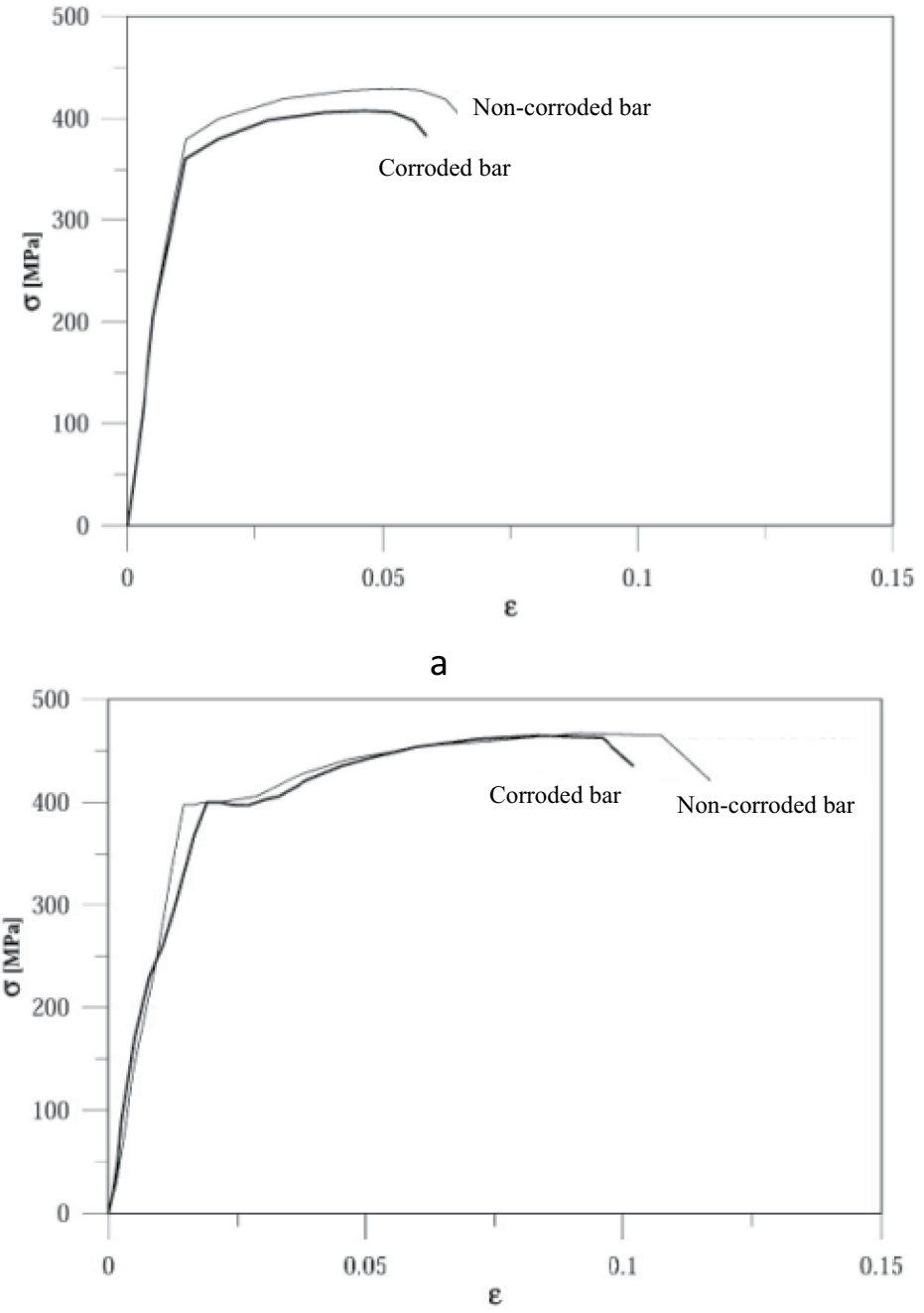

Fig. 8 Comparison of stress-strain diagrams of reinforcing bars with and without corrosion for diameters: **a** 12 mm, **b** 14 mm

individual element underwent a centered compression test, during which crack patterns and relative displacements were recorded at each load increment. To ensure uniform load distribution, a steel plate measuring 80 × 80 × 20 mm was placed between the machine and each tested specimen, as depicted in Fig. 9.

This loading method was chosen to simulate the footprint area of a bearing support related to the overall area of the pedestal, thereby assessing the influence of the load footprint area reduction compared to the block, a topic widely discussed in the literature [20, 21].

For the compression tests on the pedestals, a Zwick/Roell & Toni Technik servo-hydraulic testing machine (Fig. 9) was used, with a maximum capacity of 4000 kN. The lower crosshead consists of a cylindrical piston with a maximum stroke of 10 cm and a minimum displacement speed of 0.1 mm/mm. The 4000 kN load cell is connected to it. When the lower crosshead moves upwards, it allows the load to be

Fig. 9 Test set-up for compressive tests on pedestal

applied. In displacement control tests, displacement is managed by the machine's piston, which is equipped with an external transducer with a maximum stroke of 20 mm and a minimum speed of 0.01 mm/mm. For displacement control tests, external transducers are also used, which can be directly applied to the test specimen and have a maximum stroke of 20 mm.

Table 3 displays the ultimate loads for each tested specimen, the corresponding shortening values, and the resulting strain values. Strain was calculated as the ratio of displacement measured by the testing machine (adjusted for load plate sinking proportional to the applied load) at the height of the block. The maximum load-bearing capacity of the pedestals, considering the entire loaded area, was calculated using the concrete strength (f_c=45 MPa) and an indentation area of 400 × 400 mm, resulting in P_{max}=7200 kN. Conversely, the minimum load-bearing capacity of the pedestals, relevant to the smaller loaded area under the plate (80 × 80 mm), was calculated as P_{min}=288 kN.

Additionally, Table 3 includes strain (ε) values and corresponding displacements (δ). These results make it possible to establish the relationship between the ultimate load P_u of each specimen and the theoretical maximum load P_{max}, and also to determine the maximum shortening values.

Figure 10 presents the test results for specimens with heights *H* of 200, 300 and 400 mm. The displacements recorded by the testing machine were adjusted to remove localized effects from the load plate punching on the specimen, ensuring accurate measurement and linear distribution proportional to the machine-recorded displacements.

The specimens with a height of 200 mm exhibits plate-like behavior, with failure occurring through an intermediate mechanism between bending and punching, as illustrated in Fig. 11a). This is evident in the specimen reinforced with 10-mm bars, where four distinct independent overhangs occur. Similar behavior was observed in specimens reinforced with 12-mm, 14-mm, and 16-mm bars maintaining the same height.

In contrast, specimens with a height of 300 mm (Fig. 11b) exhibited failure through the activation of a truss mechanism, following a classical strut-and-tie behavior, regardless of the type of reinforcement used.

For all specimens with a height of 400 mm (Fig. 11c), failure occurred due to the development of vertical split cracks, following the classic mechanism of compressed diffusive regions.

2.4 Pedestals with Corroded Reinforcements

Table 4 provides the values of loads, displacements, and strains for the corroded specimens. Figure 12 illustrates the results obtained for beams with heights *H*=200, 300, and 400 mm, all with corroded reinforcement. Similar to the findings with non-corroded reinforcement, the failure modes remained consistent with the mechanisms observed in specimens of different heights.

In the presence of corrosion, a slight reduction in strength was observed. However, the authors suggest that this reduction may not be solely attributable to corrosion but could

Table 3 Peak load of uncorroded specimens

Specimen	B (mm)	H (mm)	A_f (mm^2)	Pu (kN)	δ (mm)	ε	Pu/Pmax	Pmax (kN)	Pmin (kN)
1	400	200	314.00	1178	0.26	0.0013	0.1636111	7200	288
2	400	200	452.16	1247	0.28	0.0014	0.1731944	7200	288
3	400	200	615.44	1350	0.23	0.00115	0.1875	7200	288
4	400	200	803.84	1679	0.31	0.00155	0.2331944	7200	288
5	400	300	314.00	1117	0.27	0.0009	0.1551389	7200	288
6	400	300	452.16	1002	0.28	0.0009333	0.1391667	7200	288
7	400	300	615.44	1197	0.15	0.0005	0.16625	7200	288
8	400	300	803.84	1248	0.25	0.0008333	0.1733333	7200	288
9	400	400	314.00	1135	0.11	0.000275	0.1576389	7200	288
10	400	400	452.16	928	0.46	0.00115	0.1288889	7200	288
11	400	400	615.44	1283	0.17	0.000425	0.1781944	7200	288
12	400	400	803.84	958	0.24	0.0006	0.1330556	7200	288

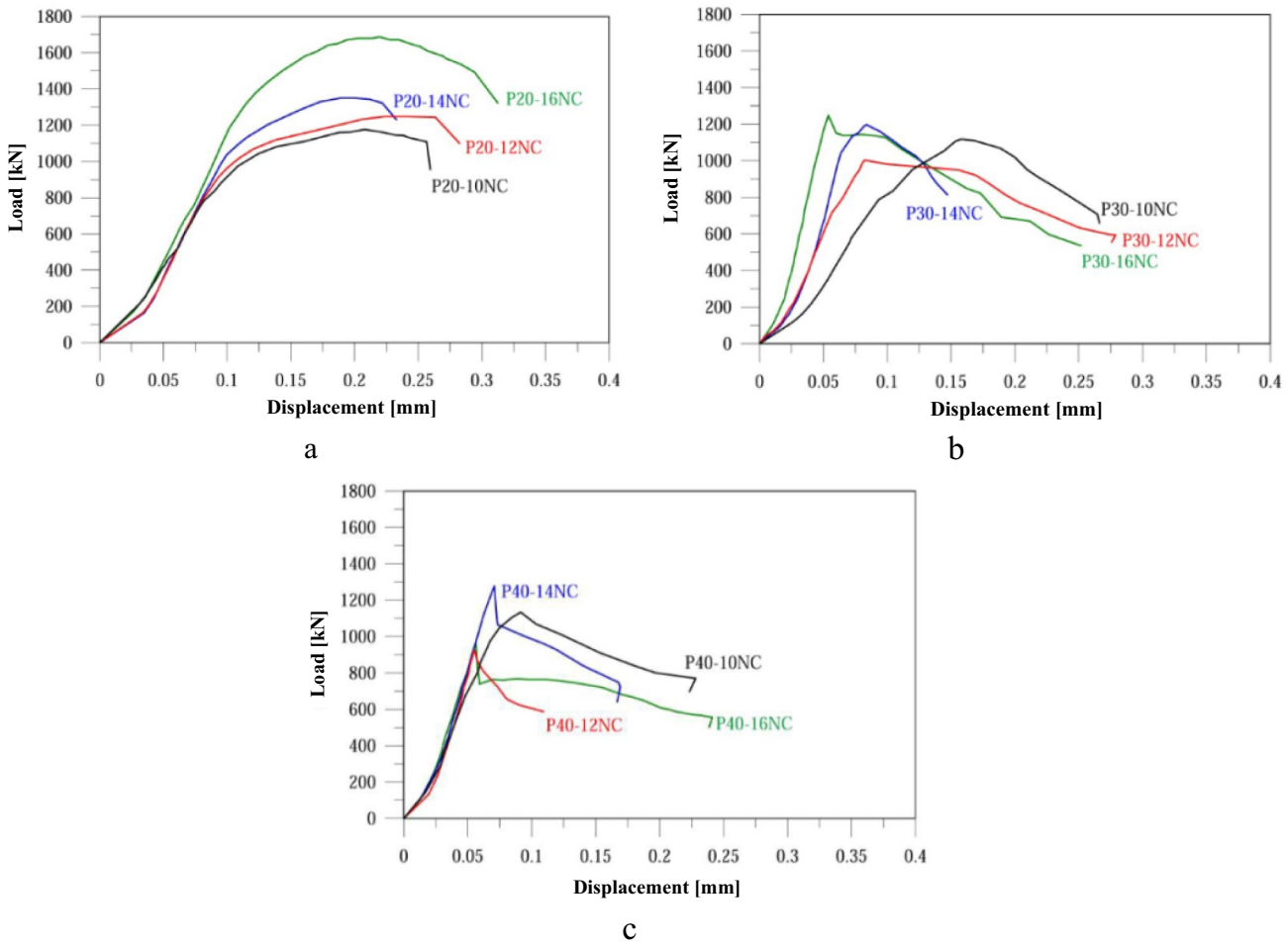

Fig. 10 Compressive tests on uncorroded specimens with height: **a** 200, **b** 300, **c** 400 mm

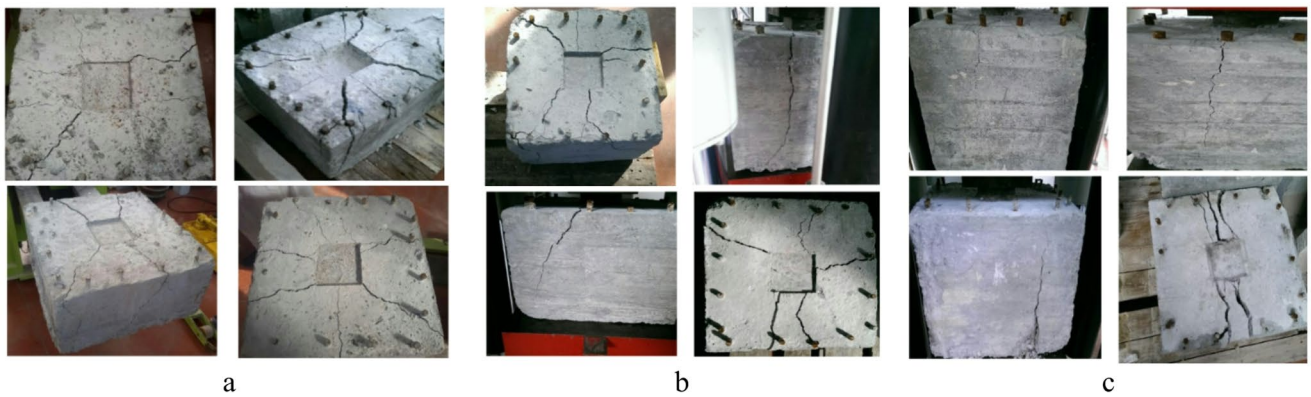

Fig. 11 Failure modes of pedestals with different heights: **a** 200, **b** 300, **c** 400 mm

also be influenced by variability in concrete strength, with the contribution of corrosion not being prominently evident.

Finally, Fig. 13 presents a comparison between non-corroded and corroded pedestal specimens. Each curve represents the average of three specimens for each series investigated. The comparison indicates that, at the stage investigated, the effects of corrosion did not lead to a significant reduction in strength. However, there was an increase in shortening at peak load, which may be attributed to concrete cracking and interface effects between steel bars and the surrounding concrete induced by corrosion.

Table 5 shows a comparison of peak loads of the pedestal specimens without corrosion and with corrosion of the

Table 4 Peak load for corroded specimens

Specimen	B (mm)	H (mm)	A_f (mm^2)	Pu (kN)	δ (mm)	ε	Pu/Pmax
1	400	200	314.0	1079	0.31	0.00155	0.149861
2	400	200	452.0	1219	0.31	0.00155	0.169306
3	400	200	615.0	1266	0.16	0.0008	0.175833
4	400	200	802.8	1440	0.29	0.00145	0.2
5	400	300	314.0	1027	0.25	0.000833	0.142639
6	400	300	452.0	954	0.3	0.001	0.1325
7	400	300	615.0	1100	0.26	0.000867	0.152778
8	400	300	802.8	837	0.27	0.0009	0.11625
9	400	400	314.0	827	0.19	0.000475	0.114861
10	400	400	452.0	845	0.15	0.000375	0.117361
11	400	400	615.0	1040	0.2	0.0005	0.144444
12	400	400	802.8	957	0.23	0.000575	0.132917

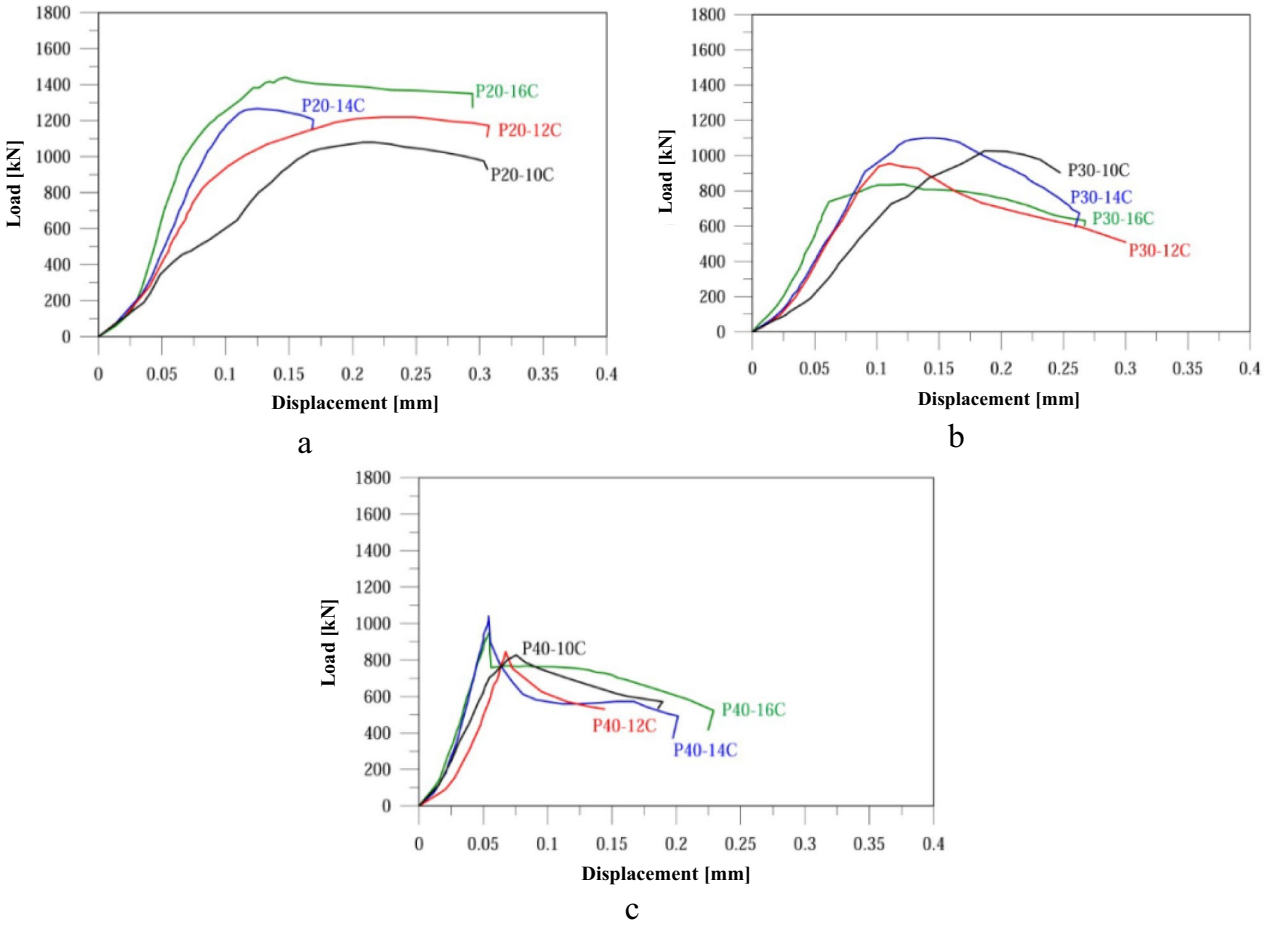

Fig. 12 Compressive tests on corroded pedestals with height: **a** 200, **b** 300, **c** 400 mm

lower bars. An average reduction in peak load of approximately 12% is observed.

From what has been observed and deduced from the results, the effect of corrosion on the peak load is not influenced by the height of the pedestal. Consequently, the same variation in ultimate load observed with different heights is registered for specimens with corroded reinforcement. Therefore, the results indicate that lower specimens carry a higher load, and excessive pedestal heights could lead to a reduction in ultimate load. Meanwhile, corrosion of the lower bars has little influence on the final result, which appears to be more affected by the cracking mechanisms rather than the reduction in area due to bar corrosion, especially when major reductions are registered in a few samples.

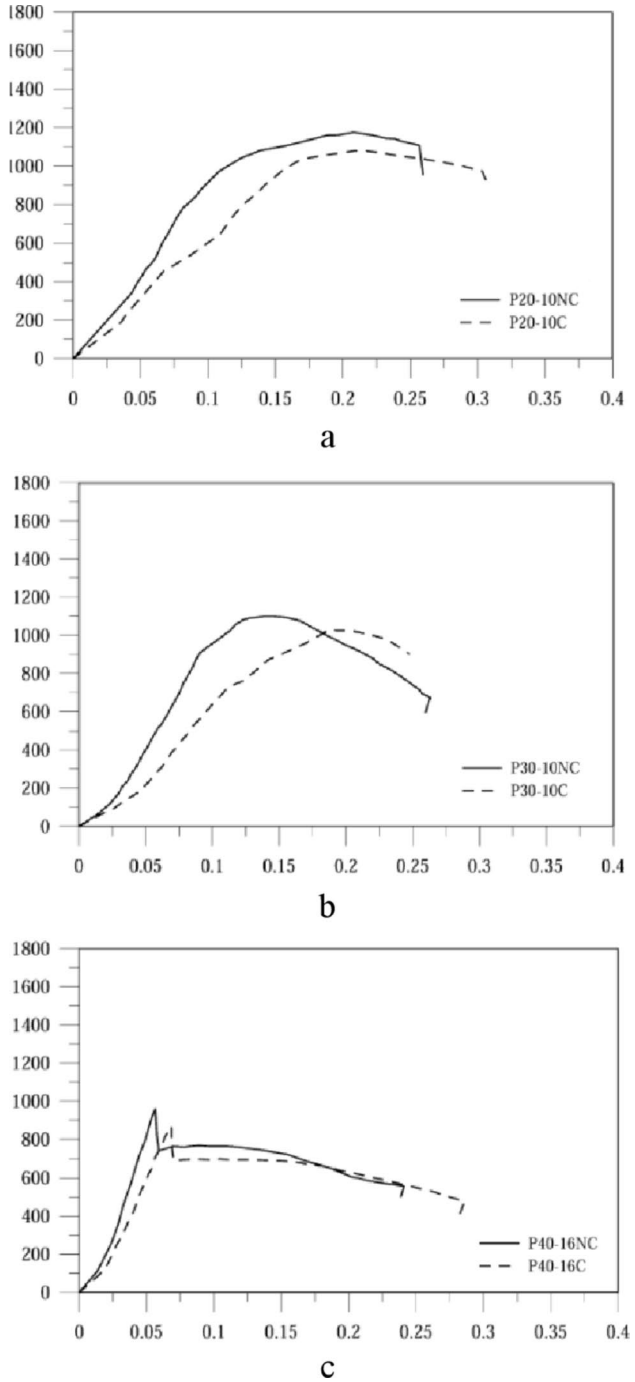

Fig. 13 Comparison of compressive tests for corroded and not corroded pedestals with height: **a** 200, **b** 300, **c** 400 mm

This result is independent of any effects of concrete confinement due to additional lateral reinforcement [22, 23]. It was decided to disregard this parameter to account for cases where corrosion of the lateral confinement reinforcement is significant and therefore its effect is negligible, but where concrete degradation occurs. Several authors have provided possible reduction coefficients for compressive stress based on the degree of concrete degradation [24, 25].

Table 5 Comparison of peak loads for non-corroded and corroded specimens

Specimen	Peak load uncorroded [kN]	Peak load corroded [kN]	Reduction of peak load
1	1178	1079	8%
2	1247	1219	2%
3	1350	1266	6%
4	1679	1440	14%
5	1117	1027	8%
6	1002	954	5%
7	1197	1100	8%
8	1248	837	33%
9	1135	827	27%
10	928	845	9%
11	1283	1040	19%
12	958	957	0%
Average reduction of peak load			12%

3 Analytical Model

Several strut-and-tie models available in the literature [25–27] can be used to calculate the cracking forces T related to the applied load P for squat elements subjected to concentrated forces on a small area with side b. One of the best-known models is the Mörsch one, illustrated in Fig. 14 from Eurocode 2 [26]. This model distinguishes between partial discontinuity (Fig. 14a) and total discontinuity (Fig. 14b).

- Partial Discontinuity (Fig. 14a): it occurs when half the height of the element is greater than the base, or when the height of the element is greater than the base.
- Total Discontinuity (Fig. 14b): it occurs when half the height of the element is less than the base, or when the height of the element is less than the base.

With reference to the geometry of the struts in Fig. 14a, when $B < H/2$, the relation between the cracking force T and the applied load P is

$$P = \frac{4 \cdot T}{1 - \frac{b}{B}} \tag{1}$$

where b is the loaded area and B the width of the element. If the cracking force is taken by the yielded steel bars, Eq. (1) becomes:

$$P_y = \frac{4 \cdot A_f \cdot f_y}{1 - \frac{b}{B}} \tag{2}$$

where A_f is the reinforcement area and f_y the steel yielding stress. In the case of a region of total discontinuity in Fig. 14b), the models were derived from the results of

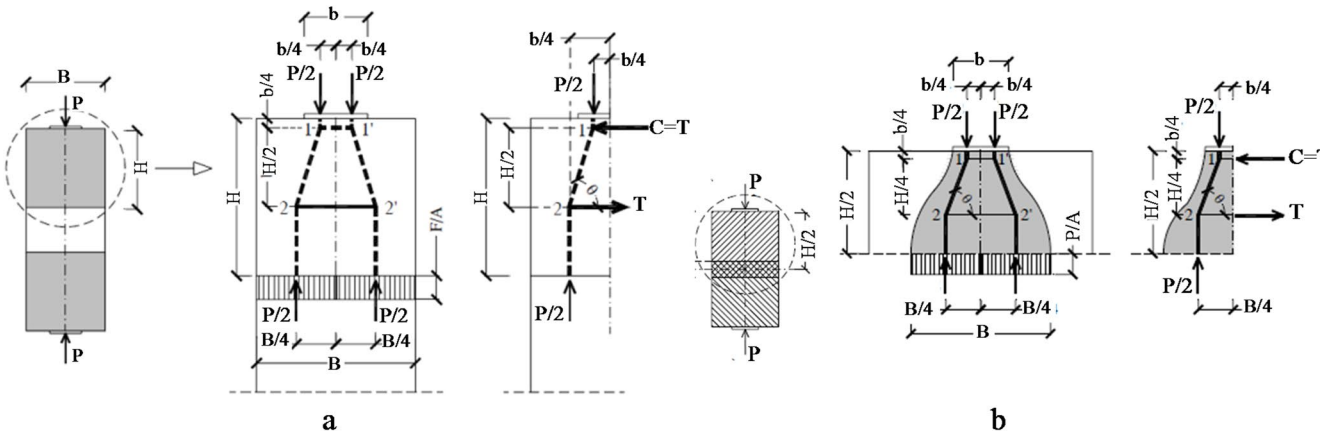

Fig. 14 Analytical model according to Mörsch. **a** partial discontinuity; **b** total discontinuity

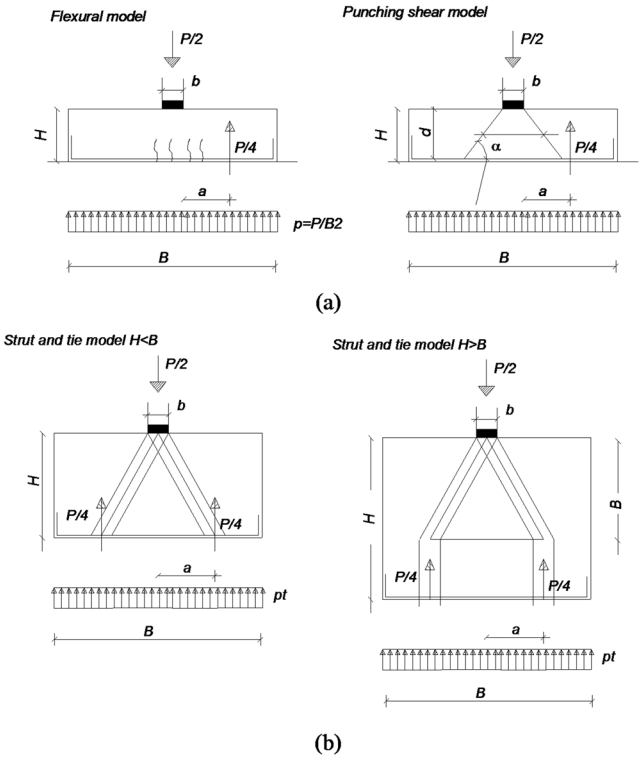

Fig. 15 Proposed strut-and-tie models for pedestals

elastic analyses conducted on two- or three-dimensional models. In this study, where the reinforcement of the pedestals is assumed to be concentrated in the lower part, it is possible to differentiate between a low pedestal ($H<<B$) exhibiting plate-like behavior, and a high pedestal ($0.5B<H<B$) exhibiting an intermediate behavior between the plate and the squat element. The reference model for the three cases examined is shown in Fig. 15.

For Fig. 15a, the flexural resistant plate model is utilized ($H<B$). In the failure condition, the four independent overhangs are loaded by the uniform load $Q=2P$. The bending resistance is given by the expression:

$$P_y = \frac{d}{\frac{B}{2} - \frac{a}{2}} \cdot 4 \cdot A_f \cdot f_y \tag{3}$$

where d is the effective depth and $a = B/4$. The punching strength is calculated here according to ACI 318 [27] with the following expression:

$$P_{u,punching} = 0.332\sqrt{f_c} \cdot 4\,(b+d) \cdot d \tag{4}$$

In the case in which $H=B$ the strut-and-tie model of Fig. 15b is assumed and the strength is equal to the minimum value between the one producing the yielding of the steel bars P_y

$$P_y = 8 \cdot \frac{d}{B-a} \cdot A_f \cdot f_y \tag{5}$$

and that producing the concrete crushing P_c:

$$P_c = 0.7 f_c \cdot b \cdot B \cdot \sin\alpha \tag{6}$$

For $H>B$, assuming $T = 0.5 \cdot \sigma_{ct} \cdot B \cdot (H-B)$ and $\sigma_{ct}=0.1\,f_c$, the value of P_c becomes:

$$P_c = 1.8 \cdot \frac{0.5 \cdot 0.1 \cdot f_c \cdot B \cdot (H-B)}{\left(1 - \frac{a}{b}\right)} \tag{7}$$

where a is the arm between the load P and the vertical component of the strut compression ($a=B/4$).

Table 6 presents the ratios between the theoretical loads calculated using the aforementioned expressions and the failure loads determined from experimental tests.

The comparison shows that the most reliable models are the proposed strut-and-tie models, particularly those predicting failure on the concrete side, as well as the Mörsch model. The comparison also reveals that the punching model agrees well with the results for specimens with $H/B=0.75$, whereas for tall pedestals, the strut-and-tie model provides

Table 6 Comparison between analytical and experimental values in terms of ratio between the analytical value of *P* and the experimental one

Specimen	Eurocode 2		Flexural	Punching	Strut-and-tie	
1	0.5198	0.5775	1.1643	0.4235	0.5198	0.7309
2	0.7071	0.7856	1.5838	0.4001	0.7071	0.6905
3	0.8890	0.9877	1.9913	0.3695	0.8890	0.6378
4	0.9336	1.0373	2.0912	0.2971	0.9336	0.5128
Average for $H/B=0.5$	0.7623	0.8471	1.7077	0.3726	0.7623	0.6430
5	0.5482	0.5392	1.8418	0.9092	0.8222	0.8954
6	0.8800	0.8655	2.9566	1.0135	1.3199	0.9982
7	1.0026	0.9862	3.3687	0.8484	1.5039	0.8356
8	1.2560	1.2354	4.2202	0.8138	1.8840	0.8015
Average for $H/B=0.75$	0.9217	0.9066	3.0968	0.8962	1.3825	0.8827
9	0.5395	0.5018	2.4168	1.5070	1.0789	0.9354
10	0.9501	0.8838	4.2565	1.8431	1.9002	1.1441
11	0.9354	0.8701	4.1906	1.3331	1.8708	0.8275
12	1.6362	1.5221	7.3302	1.7854	3.2724	1.1083
Average for $H/B=1$	1.0153	0.9445	4.5485	1.6172	2.0306	1.0038

a better interpretation of the results, both for Eurocode and the one proposed in this study, the latter being quite conservative. Finally, the flexural model is reliable only for the lowest pedestals, that is for ratios $H/B \leq 0.5$.

If the contribution of corrosion is to be considered, it is possible to include in the analytical model a reduction of reinforcement cross-section and a reduction of the compressive strength f_c, to take into account the degradation of concrete that generally accompanies advanced corrosion of the skin reinforcements, as already seen in the previous section and recommended in the literature [24, 25].

The ultimate load assessments made in Table 6 with different analytical models mainly concern the variation of the height/width ratio of the pedestal together with the variation of the lower reinforcement quantity, which seems to be less significant. The confinement of concrete is not considered here because it is assumed that it is not effective due to corrosion of the lateral bars and degradation of the concrete. Further developments of the study with new experimental investigations will also be able to consider these aspects, for non-degraded pedestals and with strong incidence of lateral reinforcement.

4 Validation Through Nonlinear Numerical Analysis

The behavior of tall and short pedestals was validated through Nonlinear Finite Element models implemented in MIDAS FEA software, with 3D block elements for concrete (average dimension of mesh 20 mm) and 1D embedded truss elements for mild reinforcements. The dead load is applied through an initial elastic analysis, and then a non-linear analysis is performed by increasing the load applied to the bearing plate. Non-linear analyses were performed following the Dutch recommendations on non-linear analyses on concrete [28]; the smeared cracking model was applied with fixed crack and secant stiffness. Concrete constitutive law in tension is modeled by an exponential law with tensile strength f_{ct} = 3.6 MPa, fracture energy G_F= 0.150 N/mm and equivalent length h = 20 mm, while the compressive constitutive law is the Thorenfeldt one with f_c = 45 MPa. Mild reinforcement steel is considered with a limited hardening branch from 390 MPa to 430 MPa. In the models shown here the bottom reinforcement is implemented with diameter φ = 12 mm.

Figure 16 shows the nonlinear FE model for H=200 mm, together with the cracking pattern. It is worth noting that in the case of H/B=0.5 (that is for H=200 mm) the failure mode is the flexural/punching one with bottom reinforcement yielded and ultimate load P_u = 1200 kN, in agreement with the average value obtained from the experimental tests and the analytical model. The average displacement in this case is δ=0.20 mm and the cracking pattern highlights this behavior with compressed concrete not crushed, open cracks at the top, bottom and side faces together with other cracks in the corners and yielded reinforcement.

In the case of H/B=1 (that is for H=400 mm) the failure mode is that of concrete crushing in the upper part of the block with widely open cracks one and ultimate load P_u = 1050 kN, in agreement with the experimental tests for which the tall pedestals show a reduced ultimate load. The average displacement is δ=0.25 mm and the cracking pattern highlights this behavior with compressed concrete crushed, open cracks at the bottom face and side faces without yielded reinforcement (Fig. 17).

The results of numerical models confirm the different failure behavior of the pedestals with different heights, obtained through tests and the reliability of analytic methods.

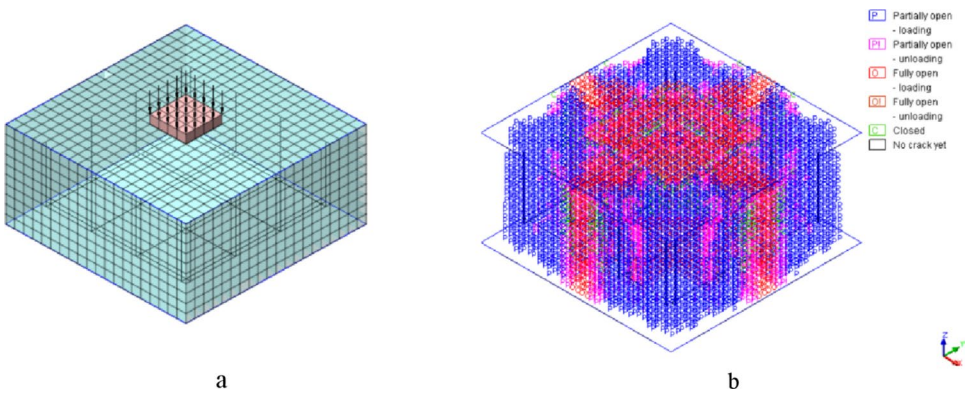

Fig. 16 Nonlinear FE analyses on pedestal model for $H/B = 0.5$. **a** Model mesh; **b** cracking pattern

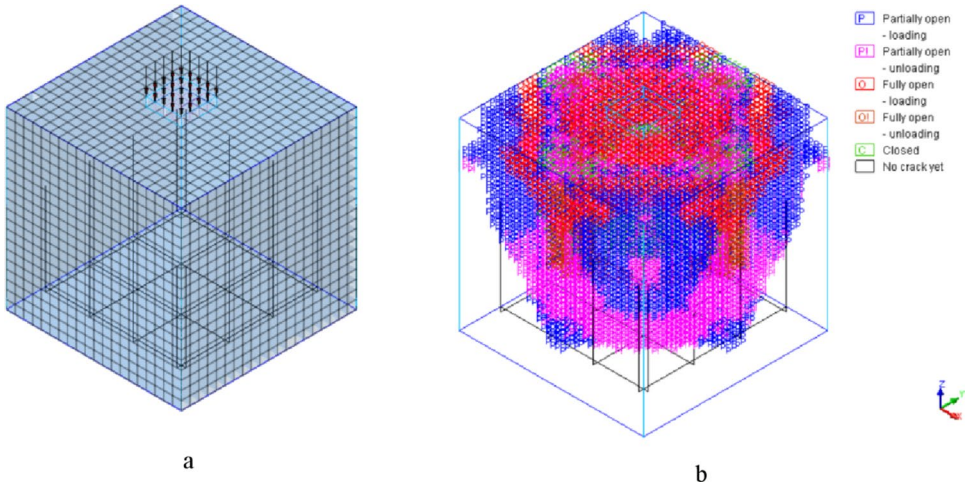

Fig. 17 Nonlinear FE analyses on pedestal model for $H/B = 1$. **a** Model mesh; **b** cracking pattern

5 Conclusions

This study investigates the theoretical and experimental behavior of reinforced concrete pedestals which play a key role in transferring loads from bridge girders to piers. Different geometric properties are considered, taking into account the possible corrosion of the bottom reinforcement. The experimental program involved testing 24 pedestals with a 400-mm base and heights of 200, 300, and 400 mm. Different percentages of reinforcement were placed at the bottom edge of the specimens, which were loaded on a reduced footprint area using steel plates measuring 80 mm in base and 20 mm in height.

Some specimens underwent artificial corrosion induced by a pitting attack over 720 days in a sodium chloride tank with a concentration of 35 g/l. Measurements of effective potential, tensile tests on both corroded and non-corroded reinforcing bars as well as crushing tests on the elements indicated that the corrosion level reached by reinforcement had a minimal impact on the strength of these elements when the reinforcement is concentrated in the lower part. This configuration optimally enhances the strength in a strut-and-tie model for squat elements.

The specimens did not suffer significant damage comparable to examples of existing structures mentioned in the introduction because the bottom reinforcement is not directly exposed, unlike the lateral or top ones (confinement and top reinforcement bars). Hence, it is possible to neglect the presence of top and lateral bars, entrusting the entire resistance of the element to the lower reinforcement in view of lower bound solutions, for which the resistant mechanism that provides the minimum safety factor is always supplied by the compressed concrete areas and the lower reinforcement in tension. The results obtained from the experimental campaign are then valid for non-corroded pedestals with negligible confinement reinforcement or corroded pedestals in which the contribution given by the top and lateral bars cannot be considered but the bottom reinforcements are still reliable as occurs for pedestals experiencing low/medium levels of corrosion typical of existing real structures during the later stages of service life. From the results the average reduction of failure load in corroded specimens is 12%.

Analytically, the study compared the Eurocode 2 model with flexural models incorporating punching and a modified strut-and-tie model proposed by the authors. It was found that the modified strut-and-tie model provides results which agrees with the experimental results, especially for

pedestals where the height equals or exceeds the base. Conversely, for shorter pedestals, the punching strength governs the structural behavior and the strut-and-tie model is no longer applicable.

The results are confirmed by numerical nonlinear analyses performed through FE models both for the ultimate load and the variability with the height/width ratio.

Future studies will explore varying dimensions of the loading area, additional steel reinforcements, and different scenarios of corrosion to further enrich the design and assessment of pedestals, especially in degraded conditions.

Funding Open access funding provided by Università degli Studi di Palermo within the CRUI-CARE Agreement.

Declarations

Conflict of interest The authors declare that they have no conflict of interest.

References

1. Bisadi V, Heada M, Cline D (2011) Seismic effects of elevating bridges with steel pedestals in the southeastern United States. Eng Struct 33:3279–3289. https://doi.org/10.1016/j.engstruct.2011.08.025
2. Hite MC, Des Roches R, Leon RT (2008) Full-Scale Tests of Bridge Steel Pedestals. J Bridge Eng ASCE 13(5):483–491. https://doi.org/10.1061/(ASCE)1084-0702(2008)13
3. Bisadi V, Gardoni P, Head M (2011) Probabilistic capacity models and fragility estimates for steel pedestals used to elevate bridges. J Struct Eng ASCE 137(12). https://doi.org/10.1061/(ASCE)ST.1943-541X.000040
4. Petrangeli MP (1996) Progettazione e costruzione di ponti. Con cenni di patologia e diagnostica delle opere esistenti (in Italian), CEA ·Editor (Rome, Italy), ISBN: 8840811591
5. Yahya NA, Dhanasekar M, Abd Hamid H (2016) Localised failure mechanism of concrete pedestals under bridge bearing. Australian J Civil Eng 18:2:164–175. https://doi.org/10.1080/14488353.2020.1752094
6. Yahya NA (2017) Strategies for mitigation of the failure of concrete pedestals supporting bridge girder bearings, Ph.D thesis at School of Civil Engineering and Built Environment Science and Engineering Faculty Queensland University of Technology Australia. https://doi.org/10.13140/RG.2.2.26864.35840
7. Zain MRM, Yahya NA, Wee LS, Lian OC, Rahman ASA (2019) Bearing Strength Behaviour of Bridge Concrete Pedestal with Confined Reinforcements. J Mech Eng 16(2):167–181. https://doi.org/10.24191/jmeche.v16i2.15335
8. Granata MF, La Mendola L, Messina D, Recupero A (2023) Assessment and strengthening of reinforced concrete bridges with half-joint deterioration. Struct Concrete 24(1):269–287. https://doi.org/10.1002/suco.202200367
9. Campione G, Granata MF, Papia M, Zizzo M (2023) Degraded Gerber Saddles in RC Bridges. J Perform Constructed Facilities ASCE 37(2):0887–3828. https://doi.org/10.1061/JPCFEV.CFENG-4016
10. Freire LM, De Brito J, Correia JR (2015) Inspection Survey of Support Bearings in Road Bridges. J Perform Construct Facilities ASCE 29(4). https://doi.org/10.1061/(ASCE)CF.1943-5509.00005
11. Granata MF, Recupero A (2015) Serviceability and Ultimate Safety Checks of Segmental Concrete Bridges through N-M and M-V Interaction Domains. J Bridge Eng ASCE. https://doi.org/10.1061/(ASCE)BE.1943-5592.0000686
12. Ince R, Arici E (2004) Size Effect in Bearing Strength of Concrete Cubes. Constr Build Mater 18(8):603–609. https://doi.org/10.1016/j.conbuildmat.2004.04.002
13. Nguyen HH, Tassoulas JL (2009) Directional Effects of Shear Combined with Compression on Bridge Elastomeric Bearings. J Bridge Eng ASCE 15(1):73–80. https://doi.org/10.1061/(ASCE)BE.1943-5592.0000034
14. Yohai L, Schreiner W, Valcarce MB, Vazquez M (2016) Inhibiting Steel Corrosion in Simulated Concrete with Low Phosphate to Chloride Ratios. J Electrochem Soc 163(13):C729–C737. https://doi.org/10.1149/2.0511613jes
15. Pedeferri P (2022) Corrosion science and engineering, Editors Luciano Lazzari and Maria Pia Pedeferri, Spinger. http://www.springer.com/series/4288
16. Robuschi S, Sumearll J, Fernandez I, Lundgren K (2021) Bond of naturally corroded, plain reinforcing bars in concrete. Struct Infrastruct Eng 17(6):792–808. https://doi.org/10.1080/15732479.2020.1768273
17. Coccia S, Imperatore S, Rinaldi Z (2016) Influence of corrosion on the bond strength of steel rebars in concrete. Mater Struct 49:537–551. https://doi.org/10.1617/s11527-014-0518-x
18. Andrade C (2018) Propagation of reinforcement corrosion: principles, testing and modelling. Mater Struct 52. 2https://doi.org/10.1617/s11527-018-1301-1
19. Imperatore S, Rinald Z, Drago C (2017) Degradation relationships for the mechanical properties of corroded steel rebars. Constr Build Mater 148:219–230. https://doi.org/10.1016/j.conbuildmat.2017.04.209
20. Ahmed T, Burley E, Rigden S (1998) Bearing capacity of plain and reinforced concrete loaded over a limited area. ACI Struct J 330–340. https://doi.org/10.14359/550
21. Markić T, Morger F, Kaufmann W (2022) Partially loaded areas in reinforced concrete: Experimental campaign and model validation. Eng Struct 273:114905. https://doi.org/10.1016/j.engstruct.2022.114905
22. Mander JB, Priestley MJN, Park R (1988) Theoretical stress–strain model for confined concrete. J Struct Eng ASCE 114(8):1804–1826. https://doi.org/10.1061/(ASCE)0733-9445(1988)114:8(1804)
23. Bonetti R, Wollmann CLR, Santos JT (2014) Bearing strength of confined concrete. ACI Struct J 111(6):1317–1327. https://doi.org/10.14359/51687163
24. Schlaich J, Schafer K, Jennewein M (1987) Towards a consistent design of structural concrete. PCI J 1987:77–150. https://doi.org/10.15554/pcij.05011987.74.150

25. Desnerck P, Lees JM, Morley CT (2018) Strut-and-tie models for deteriorated reinforced concrete half-joints. Eng Struct 161:41–54. https://doi.org/10.1016/j.engstruct.2018.01.013
26. CEN. European Committee for Standardization (2005) Eurocode 2 – Design of Concrete Structures – Part 1.1: General Rules and Rules for Buildings. CEN, Brussels, Belgium
27. ACI Committee 318 (2019) Building Code Requirements for Structural Concrete (ACI 318–19) and Commentary. American Concrete Institute, Farmington Hills, MI, p 430
28. Hendriks MAN, De Boer A, Belletti B (2017) Guidelines for Nonlinear Finite Element Analysis of Concrete Structures, Rijkswaterstaat Centre for Infrastructure, Report RTD:1016-1:2017